Andrei Rineiski
Group TRANS,
Karlsruhe Institute of Technology (KIT),
B.421, Hermann-von-Helmholtz-Platz 1,
Eggenstein-Leopoldshafen 76344, Germany
e-mail: andrei.rineiski@kit.edu

Clément Mériot
EDF-R&D, EDF Lab Paris-Saclay,
7 Boulevard Gaspard Monge,
Palaiseau 91120, France
e-mail: clement.meriot@edf.fr

Marco Marchetti
Group TRANS,
Karlsruhe Institute of Technology (KIT),
B.421, Hermann-von-Helmholtz-Platz 1,
Eggenstein-Leopoldshafen 76344, Germany
e-mails: marco.marchetti@kit.edu,
marco.marchetti@framatome.com

Jiri Krepel
Group ANS,
Paul Scherrer Institut (PSI),
Villigen 5232, Switzerland
e-mail: jiri.krepel@psi.ch

Christine Coquelet-Pascal
CEA, DES, IRESNE, DER, SPRC, LE2C,
Bat.230,
St Paul lez Durance Cedex, 13108, France
e-mail: christine.coquelet@cea.fr

Haileyesus Tsige-Tamirat
European Commission/Joint Research Centre
Petten,
Westerduinweg 3 1755 LE, Petten
e-mail: haileyesus.TSIGE-TAMIRAT@ec.europa.eu

Francisco Álvarez-Velarde
CIEMAT,
Avda. Complutense,
40. Ed. 17,
Madrid 28040, Spain
e-mail: francisco.alvarez@ciemat.es

Enrico Girardi
EDF-R&D, EDF Lab Paris-Saclay,
7 Boulevard Gaspard Monge,
Palaiseau 91120, France
e-mail: enrico.girardi@edf.fr

Konstantin Mikityuk
Group ANS,
Paul Scherrer Institut (PSI),
Villigen 5232, Switzerland
e-mail: konstantin.mikityuk@psi.ch

ESFR-SMART Core Safety Measures and Their Preliminary Assessment

A large 3600 MW-thermal European sodium fast reactor (ESFR) concept has been studied in a European Horizon-2020 project since September 2017, following an earlier European project. In the paper, we describe new ESFR core safety measures focused on prevention and mitigation of severe accidents. In particular, we propose a new core configuration for reducing the sodium void effect, introduce passive shutdown systems, and implement special paths in the core for facilitation of molten fuel discharge in order to avoid recriticalities after a hypothetical severe accident. We describe and assess the control and shutdown system, and consider options for burning minor actinides.
[DOI: 10.1115/1.4052588]

Keywords: sodium fast reactor, ESFR, sodium void effect, passive shutdown system, re-criticality prevention

1 Introduction

This paper describes new core safety measures for a 3600 MW-thermal European sodium fast reactor (ESFR) concept, studied since late 2000s in European projects. The first 4-year project was a collaborative project for a European sodium fast reactor (CP-ESFR) [1] on studies of ESFR with both mixed oxide and carbide fuels. The next project since 2017 is a Horizon 2020 project called European sodium fast reactor safety measures assessment and research tools (ESFR-SMART) [2], which continues to investigate the oxide fuel option. We refer to the initial ESFR concept with

Manuscript received August 6, 2020; final manuscript received September 15, 2021; published online October 29, 2021. Assoc. Editor: Joerg Starflinger.

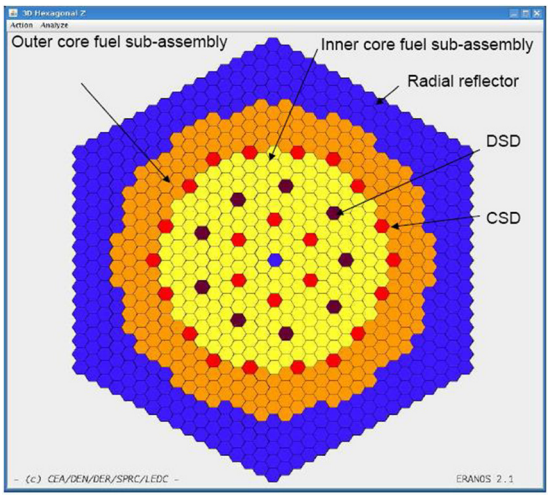

Fig. 1 ESFR-WH core: radial layout

oxide fuel of CP-ESFR as ESFR working horse (ESFR-WH) in the following.

European sodium fast reactor-WH differs from earlier large European fast core designs appreciably. Due to relatively thick pins, the fuel volume fraction is higher, and the sodium and steel volume fractions are smaller. The fertile blankets are not present. Figure 1 shows the radial core layout, including diverse shutdown devices (DSDs), and control and shutdown devices (CSDs), and a central steel subassembly. A higher fuel volume fraction leads to relatively lower enrichments of 14.6 wt % and 17 wt % in the inner and outer cores, respectively, see pin dimensions and other data for ESFR-WH in Table 1. For the considered fuel cycle with multiple recycling of plutonium, initially from spent light water reactor fuel, the breeding gain (BG) is near zero, marginally positive, and the reactivity loss under irradiation is below 1.5 $per cycle of 410 days, 1 $being the effective delayed neutron fraction, that is about 400 per cent mille (pcm) in ESFR. The sodium void reactivity effect (SVRE) is smaller in ESFR-WH than in earlier large European fast reactor designs, in particular due to a lower sodium volume fraction, but definitely positive: about 3 $ at the beginning of life (BOL), and 5 $ at the end of equilibrium cycle (EOEC). As sodium boiling may occur after a hypothetical severe accident in ESFR, a smaller SVRE is favorable for reactor safety.

In Sec. 2, we briefly review core optimization activities previously performed in CP-ESFR. In Sec. 3, we report in more detail—as compared to Ref. [3]—on new ESFR-SMART core safety measures focused on prevention and mitigation of severe accidents. In particular, we describe a new core configuration with a reduced SVRE, implementation of passive shutdown systems and special paths in the core for facilitation of molten fuel discharge. The introduction of these paths may help to avoid recriticalities and therefore to reduce the energy release after a hypothetical accident. We also assess the control and shutdown system in Sec. 4, and briefly consider minor actinide burning options in Sec. 5.

Table 1 Main ESFR-WH parameters

Number/enrichment of inner core fuel SAs	225/14.6 wt %
Number/enrichment of outer core fuel SAs	228/17.0 wt %
Number of CSDs	24
Number of DSDs	9
Target fuel residence time (effective power days)	2050
Target burn-up (GWd/t)	100
Fissile core height (cm)	100
HEX SA pitch (mm)	210.8
Fuel pellet diameter (mm)	9.43
Fuel pin outer clad diameter (mm)	10.73
Number of pins per fuel SA	271

2 Collaborative Project-European Sodium Fast Reactor Core Optimization Studies

Preliminary safety assessments did show that relatively large power excursions would be possible in ESFR-WH due to a positive reactivity variation induced by sodium boiling after a hypothetical accident. These excursions could lead to core melting, then to separation of molten steel and fuel, which are materials of different densities. This separation may lead to recriticalities caused by fuel movement [4]. The induced by recriticalities power excursions are challenging events with respect to reactor vessel integrity because of potentially strong reactivity variations due to fuel movement. A final large excursion may happen at some time and force a massive fuel discharge from the core, making then the reactor deeply subcritical, the mechanical energy release caused by this excursion being in the general case higher if more energy is accumulated in the core, mainly due to excursions happened before. In the literature, the transient progression before and shortly after the first excursion—when the intact subassembly (SA) can walls restrict the radial fuel movement—is often referred as the initiation or primary phase. The next transient phase is the transition (to full core melting) or secondary phase.

The core optimization studies in CP-ESFR addressed two issues: (1) reduction of SVRE in order to prevent or limit core damage during the initiation phase and (2) introduction of special paths for facilitation of early molten fuel discharge from the core in order to prevent multiple recriticalities during the transition phase.

2.1 Sodium Void Effect Reduction Options of Collaborative Project-European Sodium Fast Reactor. Several SVRE reduction options were investigated in CP-ESFR, including introduction of moderator materials and ways for making the core flatter, i.e., shortening the core fissile height while increasing the core diameter. A core flattening increases the neutron leakage that is favorable for SVRE reduction, but increases the core radius and the number of SAs that may increase construction and operation costs.

The most effective SVRE reductions proposed in CP-ESFR—that do not change the fissile region geometry—are based on modifications of the axial material arrangements above and below the core. A so-called sodium plenum, i.e., can walls with sodium inside, topped by an absorber layer above, replaces the steel reflector above the core. A similar approach for SVRE reduction is used in the BN-800 reactor as proposed in Ref. [5]. The idea is that sodium boiling in the core would spread to the plenum above; then the neutron leakage through the plenum would increase after its voiding, thus making SVRE less positive. An additional design modification for SVRE reduction is the introduction of a short fertile blanket instead of the steel reflector below the core; this measure facilitates neutron leakage down from the core and further reduces the void effect. The introductions of the plenum with the absorber layer above and of the fertile blanket below the core resulted in a so-called ESFR-CONF2 design, with the same radial arrangement as ESFR-WH, but with a new axial one, see Table 2. The fissile and absorber pins are separated from the sodium plenum by steel plugs, the above-fuel-plugs being shorter than in ESFR-WH in order to make the plenum more effective. SVRE, after voiding the core and plenum in ESFR-CONF2, is about 1 $ at BOL, and about 3 $ at EOEC, which is appreciably lower than SVRE in ESFR-WH.

2.2 Paths for Molten Fuel Discharge in Collaborative Project-European Sodium Fast Reactor. Also introduction of special SAs for facilitation of molten fuel discharge from the core was considered in CP-ESFR. This approach resembles a fuel SA

Table 2 Axial structure ESFR-CONF2 fuel SA: heights in cm

Head	23
Reflector	27.6
Absorber	28.2
Plug	1.8
Na plenum	60
Plug	1.8
Upper gas plenum	5
Fissile core	100
Fertile blanket	30
Lower gas plenum	91.3
Plug	8.2
Foot	37

design option called fuel assembly with inner duct structure (FAIDUS) [6].

In a FAIDUS SA, a duct with sodium inside replaces a group of fuel pins. After a hypothetical accident, molten fuel penetrates into the duct and then discharges through the duct from the core. This approach facilitates early molten fuel discharge within the SA, but makes the SA design more complex.

A modified CP-ESFR design includes, instead of many FAIDUS SAs, few molten fuel discharged tubes, i.e., can walls with sodium inside. These discharge tubes are similar to control rods without absorber, also connected to the inlet sodium plenum. This design is less complex than FAIDUS, but includes stronger obstacles, in particular the SA can walls, for molten fuel relocation. After replacement of 18 fuel SAs by the discharge tubes in the inner core, the outer core contains extra 18 fuel SAs added to the core periphery.

All discharge tubes considered in CP-ESFR are in a hexagonal ring between DSDs and external CSDs. This arrangement aims to prevent or reduce radial inward movement of the outer higher enriched molten fuel, thus decreasing the recriticality potential. The introduction of the tubes is slightly favorable for the sodium void effect: in case of sodium boiling in adjacent fuel SAs, the introduced reactivity effect is slightly smaller than the effect for the configuration with no tubes. This is because sodium remains inside the tubes and moderates neutrons around. A full tube voiding—after a hypothetical accident—results in a negative reactivity effect because of a strong neutron leakage through void tubes.

A limited number of transient simulations for modified designs in CP-ESFR preliminary confirmed [7] a better transient behavior of ESFR-CONF2 compared to ESFR-WH during the initiation phase, but did show that a further SVRE reduction would be of interest. The simulations also confirmed the possibility of molten fuel penetration into the discharge tubes, but simulation results were sensitive to sodium flow rates and temperatures inside the tubes and in the gaps between the tubes and fuel SAs.

Note that transient simulations performed by now relied on rather simplified models for accounting core geometry variations under transient conditions, such as radial core expansion models based on diagrid thermal expansion, axial core expansion models based on fuel or clad expansion. The fuel-driven option is more accurate for nonirradiated fuel. Under irradiation, the gap between fuel and clad may disappear; then the clad-driven model is more accurate. Results that take into account more complex core deformations, such as SA bowing, are not yet available, but the related uncertainties in the total reactivity feedback in the considered large system are less important than in a small reactor.

3 European Sodium Fast Reactor-Safety Measures Assessment and Research Tools Core Safety Measures

In ESFR-SMART, we continue studies performed in CP-ESFR, while taking into account core safety measures proposed for a recent design called advanced sodium technological reactor for industrial demonstration (ASTRID) [8].

A 1500 MW-thermal ASTRID sodium-cooled reactor design includes, among others, two particular features. First, the inner fissile region is shorter than the outer one. Shortening of the inner core is more efficient for void effect reduction—per eliminated fissile volume—than shortening of the full core because of a higher neutron leakage from the core periphery. Second, the inner core incorporates an axial fertile blanket at an intermediate axial position. The introduction of this blanket reduces the void effect by increasing the axial leakage of neutrons; it also improves the Pu balance and lessens the reactivity loss under irradiation.

3.1 Preliminary European Sodium Fast Reactor-Safety Measures Assessment and Research Tools Core. In ESFR-SMART we target a new core with a near-zero or negative void effect, reduced by more than 1 $ as compared to ESFR-CONF2.

The earlier studies show that an option would be a core with a shorter inner fissile region and a larger diameter: to compensate the elimination of fuel in the inner region. If the fissile height is shorter in the inner core, a reflector or fertile blanket replaces the fissile material in the inner core. We compared three different ways of introduction of a shorter fissile region and a larger nonfissile region in the inner core for ASTRID-like designs; see Fig. 2 with three configurations with the same inner fissile heights. We refer to them as (1) M0, with a fertile axial blanket at intermediate position, as in ASTRID, (2) M1, with the same blanket, but at a lower position, and (3) M2, in which the upper boundaries of inner and outer cores are at the same level, while the inner lower blanket is thicker.

Calculations [9] did show that M2 would be a promising configuration for void effect reduction is ESFR. M2 appears to be also a better option for the control rod efficiency. Another point is that a fertile material relocation after a hypothetical accident would not results in a positive reactivity introduction in M2, unlike M0, because the fertile blanket is not in a high neutron importance region. The M0 intermediate blanket increases Pu balance. In the considered by now ESFR configurations, however, the Pu balance is near zero for ESFR-WH or definitely positive in ESFR-CONF2, due to a relatively low enrichment in both configurations and a fertile blanket in ESFR-CONF2; therefore we need no augmentation of the Pu balance. One may see M2 as a core with an inner radial blanket as compared to M0 with an inner axial one.

We established an M2-like preliminary ESFR-SMART axial configuration by reducing in ESFR-CONF2 the inner fissile height from 100 to 80 cm and adding extra fuel SAs to the outer core region. Below the fissile region, we put a fertile blanket, 5 cm thick, and a steel reflector below the blanket, 40 cm and 20 cm thick, in inner core and outer core, respectively. A relatively short fertile blanket of 5 cm is to reduce the positive Pu balance.

Extra fuel SAs introduce a bit more fissile volume than the one eliminated in the inner core, thus offering more space for future optimizations. The number and locations of fuel SAs, control rods and discharge tubes, the fuel reloading scheme, and the reflector layout in plane for the preliminary ESFR-SMART core are shown in Fig. 3. This radial layout was not modified in the optimization procedure described in the following; therefore, Fig. 3 also represents the optimized ESFR-SMART core.

Because of the higher fissile region in the outer core, one may opt for the same enrichment of about 17 wt % in the inner and outer cores; this option simplifies fuel fabrication and reduces

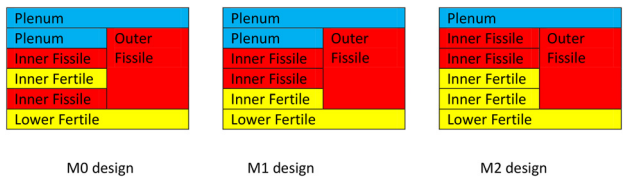

Fig. 2 M0, M1, M2 axial core arrangement options

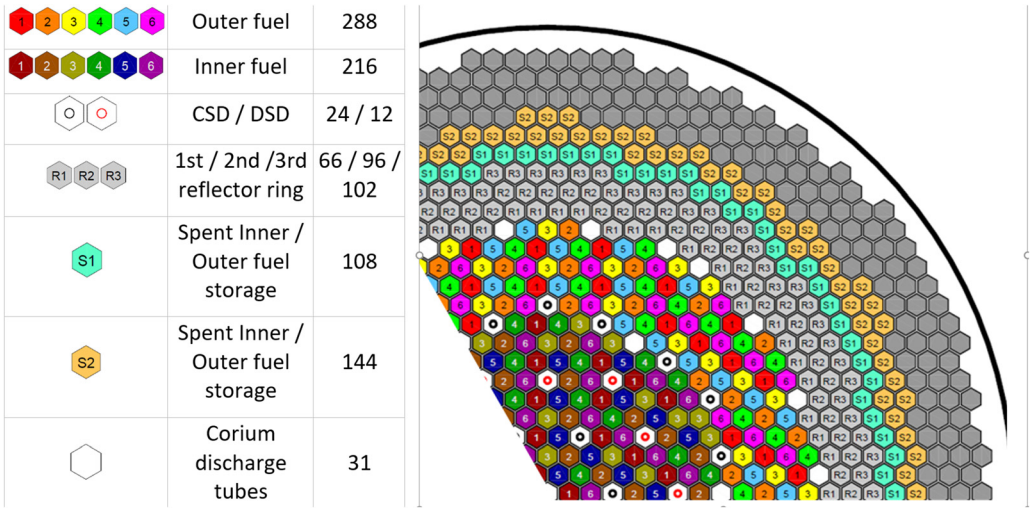

Fig. 3 ESFR-SMART radial layout and reloading scheme (120 deg symmetry)

recriticality potential due to accidental radial molten fuel movement.

The assessment of the control and shutdown system is discussed in Sec. 4. The discharge tube locations differ from those considered in CP-ESFR: 7 tubes in the inner core, including 1 central one, and 24 tubes at the core periphery. A smaller number of inner tubes helps to limit the fissile core diameter, while more tubes at the periphery offer more paths for molten fuel relocation. Unlike CP-ESFR, but similar to ASTRID, the discharge tubes in the currently considered design are connected to the core catcher that is well below the sodium inlet plenum.

For the preliminary ESFR-SMART configuration, the void effect is smaller than in ESFR-CONF2, but a further SVRE reduction is of interest. The BG is positive. Therefore, we did more effort on core optimization. As the design differs now appreciably from ESFR-WH, one should also check whether the ESFR-WH pin and SA designs are optimal for the new configuration too.

3.2 European Sodium Fast Reactor-Safety Measures Assessment and Research Tools Core Optimization. Following the preliminary work depicted in Sec. 3.1, we applied a special method called heuristic system for core design and optimization (SHADOC)-based design development system (SDDS) [10], for optimization of the preliminary configuration. The goals were to reduce SVRE further and to achieve a near-zero BG, while keeping a relatively simple design. A conventional approach to optimization studies is to proceed step-by-step, parameter after parameter, first with neutronics codes, then with thermal-hydraulics and thermal–mechanics evaluations. After a design modification, this time-consuming process is repeated. This does not ensure, however, a catch of the global optimum. The SDDS method, see Fig. 4, unlike the conventional approach, supports multiphysics analyses, dealing with neutronics, thermal-hydraulics and fuel models simultaneously, and can cover a very large parametric space, not missing any promising option.

3.2.1 Design of Experiment. With SDDS, we consider eight types of variations related to the axial and internal structure of SAs:

- variations of the fertile plate height and position in the inner core, see Fig. 5. A fertile plate height (F) augmentation reduces the steel reflector height below so that total height of the blanket and reflector is the same;
- variations of the inner/outer (D) upper fissile boundary offset;
- variations of the outer core height (H);
- variations of the pellet radius and the inner clad radius;

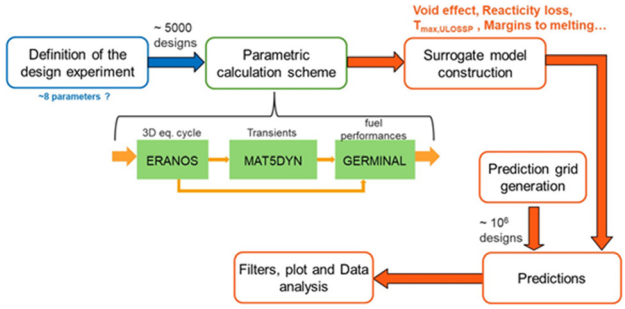

Fig. 4 General layout of the SDDS method

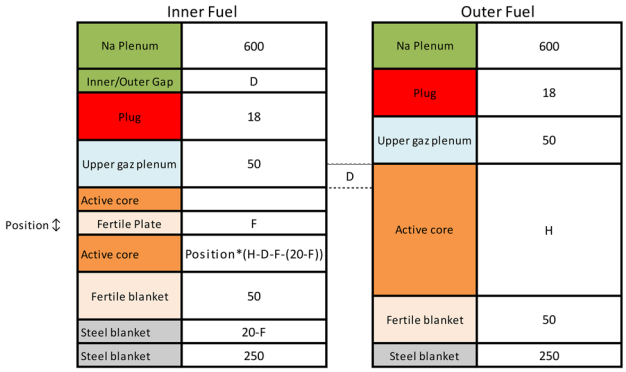

Fig. 5 Axial structure of fuel SAs and parameters used for the optimization

- variations of the spacer wire diameter;
- variations of the number of pins per SA.

With SDDS, we did proceed under constraints for the fuel pellet hole and outer clad radii, also for the number of pins in fuel SAs. A larger pellet hole radius improves core behavior after hypothetical unprotected loss of station power (ULOSSP) and unprotected control rod withdrawal (UCRW) accidents, but is limited due to other reasons. We assume that this parameter is always equal to 1/3 of the pellet radius. We also restrict core diameter augmentations — due to variations of the number of pins in SA and the pin dimensions — by 10%.

We created a 5000-points design of experiment using entropy maximization methods [11], in order to maximize the dispersion

Table 3 Ranges of the parameters

Parameters	Initial design (M2)	Min	Max
Pellet radius (cm)	0.4715	0.3	0.5
Cladding inner radius (cm)	0.4865	0.35	0.5
Spacer wire diameter (cm)	0.1	0.08	0.12
Number of pins	271	271	331
Outer core height (cm)	100	90	130
Inner/Outer height offset (cm)	0	0	30
Fertile plate position (% of inner height)	0	0	50
Fertile plate height (cm)	0	0	20

of the points over the parametric space and to improve the quality of surrogate models established afterward. Table 3 shows the variation ranges used with SDDS.

3.2.2 Calculation Scheme. For computing performances of all core configurations we used European reactor analysis optimized calculation system (ERANOS) [12], MAT5DYN [13], and GERMINAL (fuel performance code) [14] codes: for the neutronics, thermal-hydraulics, fuel performances analyses, respectively. The ERANOS calculation scheme consists of several steps, while employing a 1968-group nuclear data library and heterogeneous geometry descriptions in fuel cell calculations, and using the produced by the cell model 33-group effective cross section for core calculations.

The first step is adjustment of the plutonium content in the inner and outer cores for each design. This step ensures criticality at EOEC plus a reactivity margin set to 700 pcm. This step also minimizes the maximal subassembly power in the core. An ERANOS 3D neutron transport solver, VARIANT, is used for this step. The second step performs fuel depletion and reloading to achieve the equilibrium, using the reloading scheme shown on Fig. 3. The third step is for reactivity feedback calculations with a diffusion solver in 3D geometry, except for sodium void worth and sodium expansion effect, calculated with a transport code in 2D RZ geometry. Finally, one should establish a complete set of data for UCRW calculations with the 3D neutron transport code, including the reactivity effects and power shape swings induced by removal of individual rods.

MAT5DYN includes a multichannel description, a simplified pin thermal evaluation, and a point-kinetics model for transient simulations. It uses a single-phase description of the coolant, and an extrapolation of the coolant temperature after reaching the boiling temperature. As we only perform comparative analyses, this approximation is suitable.

Table 4 95% confidence intervals for major performance indicators

Performance indicator	2σ (95%)
SVRE (pcm)	91
Reactivity loss (pcm)	20
Nominal margin to melting (°C)	41
UCRW margin to melting (W/cm)	10
Maximal sodium temperature in ULOSSP (°C)	45
BG (%)	0.42

The thermal–mechanics calculations are performed with GERMINAL. The maximum linear power is taken from neutronics calculations. For each core configuration and for each cycle of its equilibrium campaign, the hottest subassemblies are simulated to determine the minimal margin to fuel melting at nominal conditions, and for each control rod withdrawal, the hottest fuel subassemblies are simulated to determine their linear power leading to fuel melting. The safety margin during UCRW is then evaluated as the difference between the linear power leading to fuel melting and the maximum linear heat rate at the end of the UCRW, considering the relative elevation of power calculated with MAT5DYN and uncertainties to ensure the nonmelting with 95% confidence.

3.2.3 Creation of Surrogate Models. The data basis containing the performances of ~5000 core designs is used to build surrogate models with an interpolation method called Kriging [15] (also called Gaussian process regression). This method performs interpolation without fitting, which is a proper option for treating results of deterministic codes, and generates a metamodel for predicting performances of similar configurations. It also gives information about the quality (confidence interval) of the prediction of the metamodel, which is very useful to eliminate unrealistic designs from consideration. The quality is evaluated using an independent set of designs (10% of the data basis).

After creating a first set of surrogate models, we realized that the quality of the prediction of the margin to melting at nominal conditions was very bad. In fact, the half of the data basis is composed by uninteresting designs that melt at normal operating conditions (see Fig. 6). Thus, we created a new set of 5000 designs, in which we prohibited negative margins to melting, by predicting their values for each core design with the surrogate models.

Then, the entire process has been repeated (simulations and construction of a new set of surrogate models). The accuracy (95% confidence intervals) values of the main surrogate models after this second step are given in Table 4.

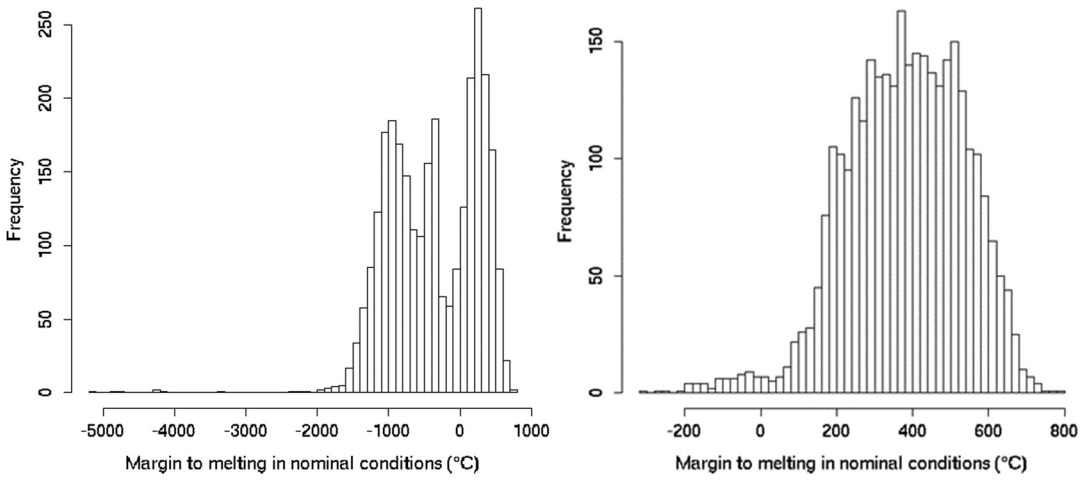

Fig. 6 Distribution of the margins to melting in nominal conditions in the first (left) and optimized (right) data basis

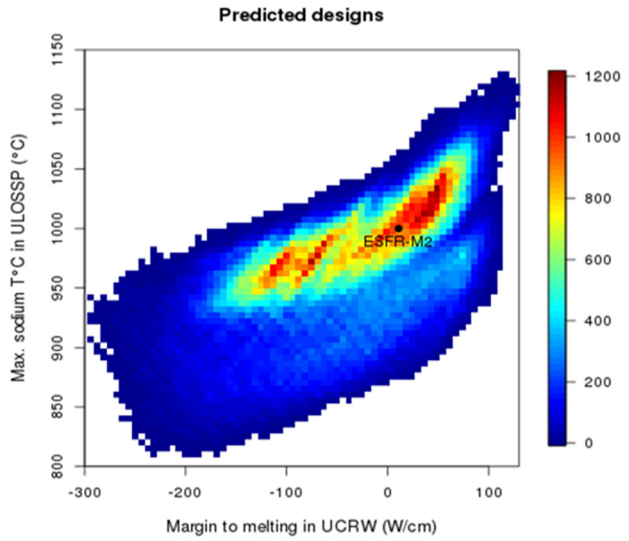

Fig. 7 Distribution of the predicted designs in the (ULOSSP-temperature, UCRW-margin) space

3.2.4 Predictions and Selection. The performances of a large amount of cores ($\sim 1.5 \times 10^6$ designs) distributed on a regular grid are evaluated with the surrogate models. Figure 7 presents the distribution of these designs in the (Maximal sodium temperature in ULOSSP, Margin to melting during UCRW) space. The preliminary ESFR-SMART design is denoted as ESFR-M2 in this and next figures. We refer to this space as (ULOSSP temperature, UCRW margin) in the following. First, we removed the nonviable cores, i.e., the ones that present a very low margin to fuel melting at nominal conditions.

The ULOSSP temperature indicator is an evaluation of the maximal temperature of the sodium, with an extrapolation when it exceeds the boiling temperature. A positive UCRW-margin value means nonmelting of the fuel after UCRW.

Then, we analyzed the distribution of the performances in this (ULOSSP temperature, UCRW margin) space and filtered the most interesting designs. Figure 8 presents the total void effect at EOEC for the predicted designs limited to the most interesting area of the space, namely, where the UCRW margin is positive. In this visualization, the color of the pixel is indexed to the mean of the performance (or parameter) of the core designs in the pixel. As we can see, we can find designs on the (ULOSSP temperature, UCRW margin) Pareto front (bottom-right frontier of the colored surface) with a very low void effect. The Pareto front shows graphically the set of Pareto-efficient options, an option being Pareto-efficient if no gain is possible in one respect without losses in other ones.

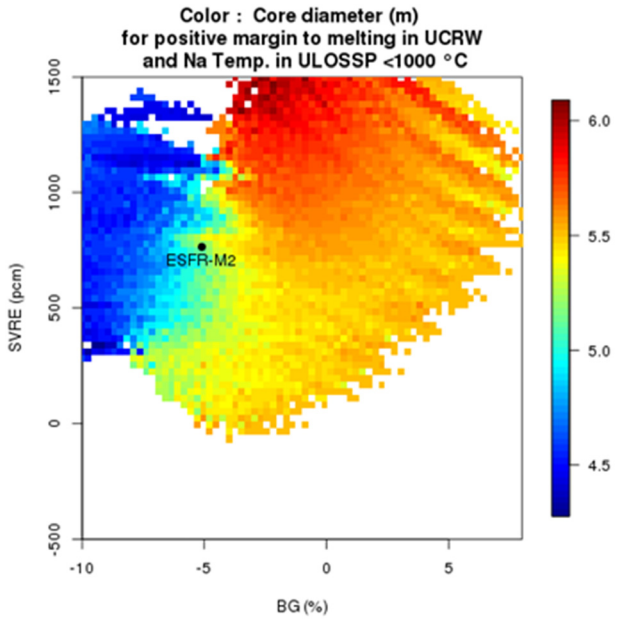

Fig. 9 Distribution of the core diameter of the predicted designs in the (SVRE, BG) space

Figure 9 shows the distribution of the core diameter of the predicted designs in the (SVRE, BG) space. Beforehand, we filtered the designs to get rid from those with nonacceptable UCRW margins and ULOSSP temperatures. This illustration shows that it is not possible to reduce the core diameter if we target a near-zero BG. Finally, designs that have a low void effect and a near-zero BG have a core diameter around 5.5 m, as well as the preliminary configuration.

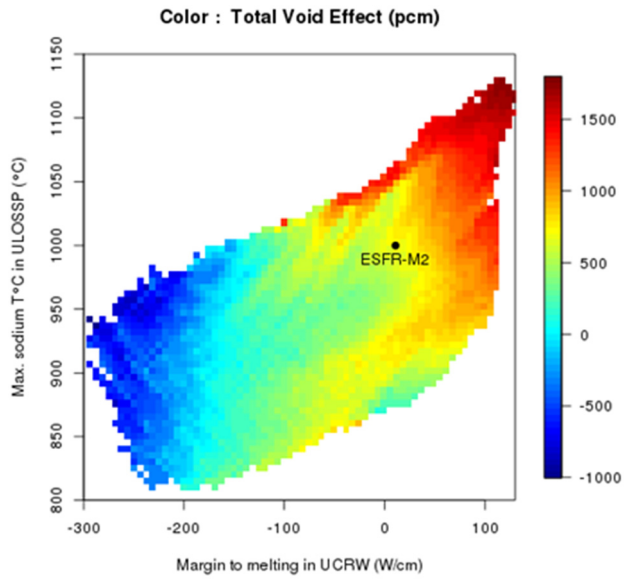

Fig. 8 Distribution of Total SVRE for the predicted designs in the (ULOSSP temperature, UCRW-margin) space

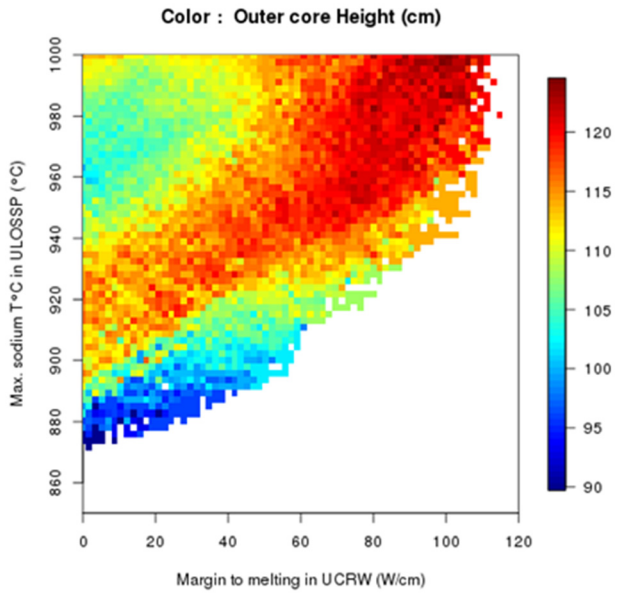

Fig. 10 Distribution of the outer core height in the (ULOSSP-temperature, UCRW-margin) space

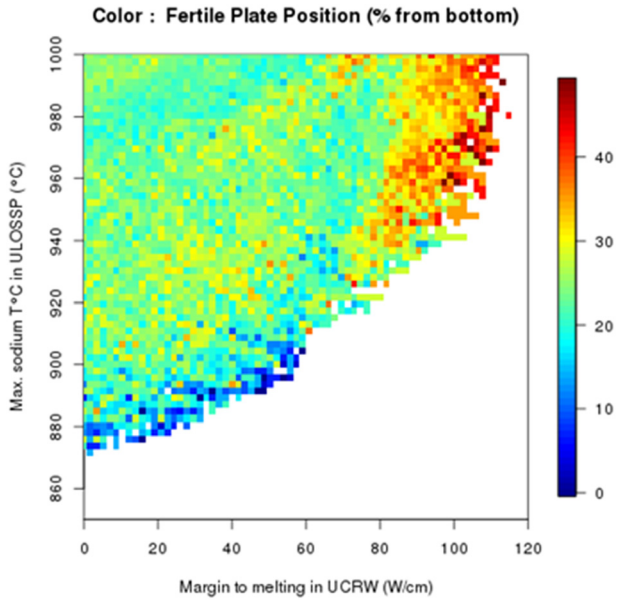

Fig. 11 Distribution of the fertile plate position (in % of the inner fuel height) in the (ULOSSP-temperature, UCRW-margin) space

Some trends have been assessed while looking at the distribution of the parameters in the (ULOSSP temperature, UCRW margin) space (see example in Figs. 10 and 11):

- The position of the fertile plate changes along the Pareto front: a higher plate is preferable to reduce the axial power form factor and improve the UCRW behavior. In this study, it is preferable to have a low fertile plate, in order to reduce the sodium void effect. Moreover, it is possible to find designs with a low fertile plate and a positive margin to melting during ULOSSP.
- Adding an upper inner/outer height offset between 0 and 5 cm improves both ULOSSP and UCRW cases. However, it is possible to find designs with satisfying performances and no offset.
- The outer core height should be reduced to improve the void effect and thus the ULOSSP temperature. However, having a near-zero BG implies to have a height of about 95 cm or higher for these designs.
- The pellet diameter must be reduced.
- The spacer wire diameter should be reduced: it is a win-win parameter for both ULOSSP and UCRW. However, for reasons of technical feasibility of the assembly, we decided to maintain the wire/pin diameter ratio above 0.09, as in CP-ESFR.
- The optimal value for the pellet-cladding gap is around 0.015 cm for these designs.

To select the most attractive designs among the predictions, we capture the successive Pareto fronts (lower right boundary on Fig. 8) and exclude the cores with a too low (<−2%) BG, a too large diameter, or with no margin to melting in case of UCRW. Then, we measure the performances of these selected designs with the ERANOS/MAT5DYN/GERMINAL scheme, to eliminate the prediction error of the surrogate models.

The design with the lowest void effect and a near-zero BG was obtained and denoted as A in Table 5, but the selected design (B) was chosen after filtering the data basis to respect some constraints of the project. Design B is the core that presents the almost lowest void effect, with a low fertile plate, a unique fuel enrichment, no inner/outer height offset, and a pooling of the axial elevations of the inner and outer fuel SAs to simplify the axial structure. Compared to the preliminary configuration, a reduction of 80% of the total void effect has been performed, while achieving a near-zero BG and slightly reducing the assembly pitch. Note that Design B is similar to M2 (as shown in Fig. 2), that confirms that a M0-type configuration with an internal axial inner blanket is not optimal for ESFR. Compared to the preliminary ESFR-SMART configuration, in the optimal one, the enrichment is increased by about 1%, to ca. 18 wt %, the fissile heights are reduced by 5 cm in the inner and outer cores, and the fertile height below the inner core is increased by 20 cm at the expense of the steel reflector below.

4 European Sodium Fast Reactor-Safety Measures Assessment and Research Tools Control and Shutdown System

Two types of absorber rod SAs are considered for the shutdown system of the ESFR: the CSD and the DSD. Both absorber rods consist of two enrichment zones: B_4C Nat. (lower part 45 cm) and B_4C 90% (upper part 40 cm CSD and 50 cm DSD). The total subassembly height is 409 cm. These control rod designs were taken from the previous CP-ESFR project.

Figure 12 shows the layout of the ESFR-SMART core with the position of the control rod subassemblies. There are in total 24 CSD rod located in the inner core (6 SA) and at the inner periphery of the outer core (18 SA). There are 12 DSD rods located in

Table 5 Performances of the preliminary and optimized designs

	Preliminary (M2)	A	B (Selected)
Inner core enrichment	17(wt %)	17.86 (vol %)	17.32 (vol %) = 17.99 (wt %)
Outer core enrichment	17(wt %)	16.93(vol %)	17.32 (vol %) = 17.99 (wt %)
Cycle length (effective power days)	2195	2170	2170
BG	−5.2%	−0.9%	−0.5%
Extended SVRE (pcm) at EOEC	765	20	153
Estimated maximal sodium Temperature in ULOSSP (°C)	>1000 (extrapolation)	761	880
Minimal margin to melting in UCRW (W/cm)	11	27	23
Outer fissile height (cm)	100	102.5	95
Inner fissile height (cm)	80	67.5	75
Outer/inner core offset (cm)	0	15	0
Fertile plate height (cm)	—	17.5	20
Fertile plate lower boundary in the inner fissile(cm)	—	0.0	0.0
Fertile blanket height (cm)	5	5	5
Inner core steel blanket (cm)	45	27.5	25
Pellet radius (cm)	0.4715	0.4680	0.4680
Cladding inner radius (cm)	0.4865	0.4835	0.4835
Fuel pellet inner hole radius (cm)	0.125	0.156	0.156
Wire diameter (cm)	0.10	0.10	0.10
Assembly pitch (cm)	21.08	20.985	20.985

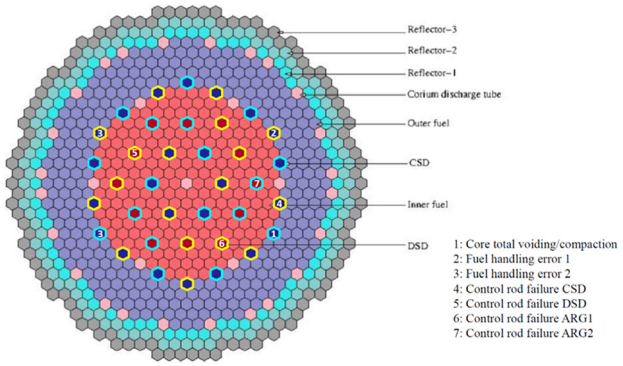

Fig. 12 ESFR-SMART core layout. The two shutdown groups of absorbers are highlighted with a yellow hexagon (ARG1) and blue hexagon (ARG2). Numbers correspond to the position of the control rod involved in the different reactivity margins. These positions have been calculated as the control rod with largest neutron flux in each case.

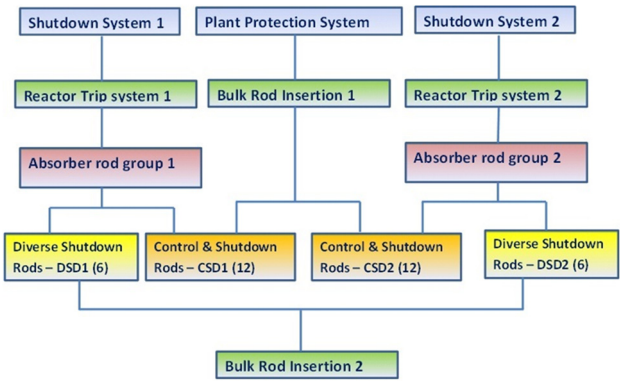

Fig. 13 ESFR-SMART shutdown system layout

the inner core, more than in ESFR-WH because of a larger number of fuel SAs and a stronger reactivity loss per cycle, evaluated in preliminary calculations reported earlier, mainly because of a higher core enrichment. The distribution of the control rod subassemblies in the core intends to enable uniform power and reactivity control in all operational and accident conditions.

The criticality calculations for the shutdown system assessments were performed using the Monte Carlo Code MCNP [16] in a heterogeneous three-dimension ESFR core model; continuous energy cross section data from the joint evaluated fission and fusion nuclear data library version 3.1 (JEFF 3.1) [17] were used in all calculations.

4.1 Shutdown System Layout. Based on past European experience [18], the described in the following shutdown system architecture has been proposed for ESFR (see Fig. 13). The reactor shutdown function in ESFR is assured by three independent, diverse, and redundant reactor shutdown systems to be designed following a defence-in-depth approach considering single failure criteria. The shutdown systems 1 and 2 are gravity driven, whereas the plant protection system uses drive motor. Each shutdown system is composed of absorber rod group 1 (ARG1) or absorber rod group 2 (ARG2), each consisting of 12 (9 in the outer core + 3 in the inner core) CSD and 6 DSD control rod subassemblies. Each absorber rod group is connected to a separate trip system and is sufficient to shut down the reactor. In order to improve the reliability of the shutdown system, envisaged is an optical link between the two absorber rod groups, which allows the actuation of one rod group to trigger the other one [15]. In addition, the DSD control rod subassemblies belong to an additional passive shutdown system, which is implemented either as self-actuated Curie point-type or hydraulically suspended.

Each group of control rods achieves adequate scram reactivity margin. Table 6 shows the calculated reactivity margins using direct eigenvalue method. For the case of total sodium draining, there is a large negative reactivity margin. The calculated reactivity margin in the case of core compaction is significantly lower than the normal shutdown margin.

Two cases were considered to assess the reactivity insertion due to fuel handling error with one and two stuck rods replaced by fuel assemblies. The reduction in reactivity margin due to fuel handling error is rather large. To estimate the reactivity margins, several calculations were performed while considering reactivity insertion mechanisms due to whole core sodium draining, core compaction, and fuel handling errors assuming that both groups of control rods are fully inserted discounting for stuck rod condition.

At cold shutdown state, the total reactivity worth of both control rod groups is −4780 pcm (ca. 12.5 $), which appears adequate to deliver sufficient subcriticality reserve to ensure reactor scram considering the various potential failure mechanisms.

4.2 Shutdown Margins. The reactivity reserve available following a reactor scram from any operational state and considering the stuck rod condition is referred to as the shutdown margin. It constitutes the negative reactivity required to shut down the reactor and to provide reactivity hold-down to maintain subcriticality over a prolonged period with an adequate reactivity margin.

Two sets of calculations were performed at the hot standby temperature (450 °C) in order to estimate the shutdown margins for the cases of reactor scram using CSD/DSD rods and ARG1/ARG2 rods.

The results of the calculations are listed in Table 7. The shutdown margins shown for both shutdown systems appear adequate. The higher reactivity worth of the CSD rods is due to the design requirements, which include a capability to compensate for the excess reactivity and for other reactivity feedbacks including refueling worth uncertainties.

The DSD rods have to provide only redundant safety shutdown capability to bring the reactor to zero power at the hot standby temperature from any operation condition considering a stuck rod fault. The reactivity reduction due to the stuck rod fault is for CSD systems in the range of 1 $ while for the DSD system it is only 0.35 $. For the outer CSD rods, the value is of the order of 1 $, thus requiring a modification of the absorber material enrichment to adjust the worth distribution between the inner and outer rods of the CSD system.

Results for the ARG1 and ARG2 system show the same level of shutdown margin. The reactivity reduction due to the stuck rod fault in this case is in the range of 130–150 pcm.

Table 6 Subcriticality reactivity margin

Reactor core—cold shutdown	Shutdown system	Reactivity margin (pcm)
Core total voiding	ARG1 + ARG2 – 1 stuck rod + void reactivity	−4138
Core compaction	ARG1 + ARG2 – 1 stuck rod + reactivity	−2743
Fuel handling error 1	ARG1 + ARG2 – 1 stuck rod + 1 Fuel SA instead of CS	−2312
Fuel handling error 2	ARG1 + ARG2 – 2 stuck rod + 2 Fuel SA instead of CS	−2040

Table 7 Shutdown reactivity margins

Reactor core—safe shutdown	Shutdown system	Reactivity margin (pcm)
Scram	CSD	−3956
	DSD	−1359
Control rod failure	CSD—1 stuck rod	−3567
	DSD—1 stuck rod	−1249
Scram	ARG1	−2701
	ARG2	−2712
Control rod failure	ARG1—1 stuck rod	−2570
	ARG2—1 stuck rod	−2566

Table 8 Reactivity insertion due to inadvertent control rod withdrawal

Control rod system		Reactivity (pcm)
CSD	Inner	147
	Outer	362
DSD		141

4.3 Accident Situations. Considerations related to inadvertent reactivity insertion play a key role in connection with the shutdown systems design requirements. There are various potential reactivity insertion mechanisms, which need to be considered to provide provisions to prevent reactivity fault accidents. For preliminary assessment performed within the present analysis, however, it is sufficient to consider an enveloping insertion mechanism such as the inadvertent withdrawal of the control rod with the highest worth. However, it has to be noted that the control rod drive mechanism has provisions to avoid any inadvertent control rod withdrawal.

The reactivity insertion due to inadvertent withdrawal of the highest worth control rod was estimated by the direct eigenvalue method. The results are shown in Table 8 for both CSD and DSD control rod withdrawal cases.

The reactivity insertion due to withdrawal of one inner CSD control rod is in the order of 140 pcm. The DSD control rod withdrawal reactivity insertion is in the same range. What is of concern is the large reactivity insertion due to the withdrawal of outer CSD control rod.

It needs to be further analyzed if this high withdrawal reactivity insertion could be a safety issue. Furthermore, additional calculations are needed to confirm that the calculated reactivity insertions could cause fuel melting and the consequences thereof.

5 Options for Minor Actinide Incineration

In the optimized ESFR-SMART design, the Pu balance is near-zero, but the Minor Actinide (MA) one is positive. On the other hand, this design includes a lower blanket that is 25 cm thick below the inner fissile region of 75 cm and is 5 cm thick below the outer one of 95 cm. This blanket can be used for MA incineration without strong influence on core characteristics. One may put in this blanket a mixture of uranium and MA oxides, e.g., with the 80-to-20 ratio, instead of uranium oxide only. Preliminary analyses [19] show that such design modifications may lead to a negative MA balance, while SVRE is slightly reduced because of a higher leakage from the core to the blanket that is a stronger absorber after MA introduction. After this modification, however, the Pu balance becomes more positive. Additional studies would be needed in order to assess in more detail options for MA incineration in the ESFR-SMART and associated fuel cycle.

6 Concluding Remarks

A large European sodium fast reactor concept has been studied in European projects since late 2000s. In the initial ESFR design, the fuel pins are relatively thick, the fuel volume fraction is relatively high, the steel and sodium ones are relatively low, that leads to lower enrichments, lower reactivity losses per cycle, and lower sodium void effect reactivity values compared to earlier large European designs. This new design approach supports an optimal utilization of plutonium from spent nuclear fuel. It is also beneficial for reactor safety.

New core safety measures were proposed in CP-ESFR and ESFR-SMART. In particular, a sodium plenum above the core and a fertile blanket below the core were introduced in CP-ESFR for sodium void effect reduction. In addition, the introduction of special tubes for molten fuel discharge in order to prevent multiple recriticality events after a hypothetical severe accident was studied in CP-ESFR.

In ESFR-SMART, we took into account earlier studies and establish a new design. A core with different fissile heights in the inner and outer regions, but with the same upper fissile axial boundary is proposed. The core is optimized with respect to safety and Pu balance by employing a new automated procedure that allows considering a very large number of design options. The fuel enrichment has been fixed to the same value in the inner and outer core regions, offering advantages for fuel fabrication and safety. The void effect was reduced to a near-zero value. On the other hand, the enrichment is higher, and the reactivity loss per cycle is stronger than in the initial ESFR design.

Finally, passive shutdown systems were introduced, and a new arrangement for discharge tubes is employed. The control and shutdown systems assessment was performed, as well as the preliminary assessments on minor actinide incineration.

The new ESFR-SMART design is expected to demonstrate better safety performances. It offers a good basis for ESFR-SMART studies and later projects.

Funding Data

- Euratom Research and Training Program 2014–2018 (Grant Agreement No. 754501; Funder ID: 10.13039/100010687).

Nomenclature

ARG = absorber rod group
ASTRID = advanced sodium technological reactor for industrial demonstration
BG = breeding gain
BOL = beginning of life
CP-ESFR = collaborative project for a European sodium fast reactor
CSD = control and shutdown device
DSD = diverse shutdown device
EOEC = end of equilibrium cycle
ESFR = European Sodium Fast Reactor
ESFR-SMART = European Sodium fast reactor safety measures assessment and research tools
ESFR-WH = ESFR working horse
FAIDUS = fuel assembly with inner duct structure
jeff 3.1 = joint evaluated fission and fusion nuclear data library version 3.1
MA = minor actinide
pcm = per cent mille
SDDS = SHADOC-based design development system
SVRE = sodium void reactivity effect

References

[1] Fiorini, G. L., and Vasile, A., 2011, "A. European Commission - 7th Framework Programme: The Collaborative Project on European Sodium Fast Reactor (CP ESFR)," Nucl. Eng. Des., **241**(9), pp. 3461–3469.

[2] Mikityuk, K., Girardi, E., Krepel, J., Bubelis, E., Fridman, E., Rineiski, A., Girault, N., Payot, F., Buligins, L., Gerbeth, G., Chauvin, N., Latge, C., and Garnier, J.-C., 2017, "ESFR-SMART: New Horizon-2020 Project on SFR Safety," International Conference on Fast Reactors and Related Fuel Cycles (FR17), Yekaterinburg, Russia, June 26–29, Paper No. 245, p. 10.

[3] Rineiski, A., Meriot, C., Marchetti, M., and Krepel, J., 2018, "Core Safety Measures in ESFR-SMART," Proceedings of PHYSOR Conference, Cancun, Mexico, April 22–26, pp. 3401–3412.
[4] Rineiski, A., Flad, M., Gabrielli, F., and Vezzoni, B., 2017, "Fast Reactor Systems in the German P&T and Related Studies," International Conference on Fast Reactors and Related Fuel Cycles (FR17), Yekaterinburg, Russia, June 26–29, Paper No. 487, p. 10.
[5] Matveev, V., Bobrov, S., Bakhlaev, I., Vorotyntsev, M., Danilytchev, A., and Eliseev, V., 1990, "Physical Grounds for Further Improvement of Fast Sodium Reactor Safety," Proceedings of the International Fast Reactor Safety Meeting, Snowbird, UT, Vol. 2, Aug. 12–16, p. 5.
[6] Kubo, S., 2012, "A Safety Design Approach for Sodium-Cooled Fast Reactor Core Toward Commercialization in Japan," IAEA, Vienna, Austria, accessed Oct. 20, 2021, https://inis.iaea.org/collection/NCLCollectionStore/_Public/45/084/45084449.pdf
[7] Rineiski, A., Vezzoni, B., Zhang, D., Chen, X.-N., Gabrielli, F., and Marchetti, M., 2011, "Sodium Void Effect Reduction and Minor Actinide Incineration in ESFR," Trans. Am. Nucl. Soc., **104**, pp. 720–721.
[8] Chanteclair, F., Rodriguez, G., Hamy, J.-M., Dupraz, R., 2017, "ASTRID Reactor: Design Overview and Main Innovative Options for Basic Design," IAEA International Conference on Fast Reactors and Related Fuel Cycles (FR17), Yekaterinburg, Russia, June 26–29, Paper No. CN-245.
[9] Gabrielli, F., 2017, Personal communication.
[10] Barjot, F., Schmitt, D., and Venard, C., 2014, "Multi-Physics and Multi-Objective Optimization Methodology for Sodium-Cooled Fast Reactor Conception," International Congress on Advances in Nuclear Power Plants (ICAPP 2014), Charlotte, NC, Apr. 6–9, p. 10, Paper No. 14176.
[11] Shewry, M. C., and Wynn, H. P., 1987, "Maximum Entropy Sampling," J. Appl. Stat., **14**(2), pp. 165–170.
[12] Rimpaul, G., Plisson, D., Tommasi, J., Jacqmin, R., and Rieunier, J.-M., 2002, "The ERANOS Code and Data System for Fast Reactor Neutronic Analyses," International Conference on the New Frontiers of Nuclear Technology (PHYSOR 2002), Oct. 7–10, Seoul, South Korea, No. cea-023906396.
[13] Massara, S., Tommasi, J., Vanier, M., and Köberl, O., 2005, "Dynamics of Critical Dedicated Cores for Minor Actinide Transmutation," Nucl. Technol., **149**(2), pp. 150–174.
[14] Roche, L., and Pelletier, M., 2000, "Modelling of the Thermomechanical and Physical Processes in FR Fuel Pins Using the GERMINAL Code," International Symposium on MOX Fuel Technologies for Medium and Long-Term Deployment, IAEA, Vienna, Austria, May 17–21, Paper No. IAEA-SM-358/25.
[15] Marrel, A., Iooss, B., van Dorpe, F., and Volkova, E., 2008, "An Efficient Methodology for Modeling Complex Computer Codes With Gaussian Processes," Comput. Stat. Anal., **52**(10), pp. 4731–4744.
[16] X-5 Monte Carlo Team, 2003, *MCNP–A General Monte Carlo N-Particle Transport Code, Version 5*, Vol. I, Overview and Theory, Los Alamos National Laboratory, Los Alamos, NM, Report No. LA-UR-03-1987.
[17] Koning, A., Forrest, R., Kellett, M., Mills, R., Henriksson, H., and Rugama, Y., eds., 2006, "The JEFF-3.1 Nuclear Data Library," OECD, Paris, France, accessed Oct. 20, 2021, https://www.oecd-nea.org/dbdata/nds_jefreports/jefreport-21/jeff21.pdf
[18] Millington, D. N., 1991, "The EFR Reactor Protection System and Third Shutdown System for Risk Minimization," International Atomic Energy Agency, IAEA-IWGFR Specialists' Meeting on Passive and Active Safety Features of LMFRs, Nov. 5–7, O-arai, Japan, p. 139.
[19] Marchetti, M., and Rineiski, A., 2018, "Minor Actinide Balance Reduction in ESFR-SMART," J. Phys. Conf. Ser., **1133**(1), p. 012027.